Report

Current Biology

Rapid Coral Decay Is Associated with Marine Heatwave Mortality Events on Reefs

Graphical Abstract

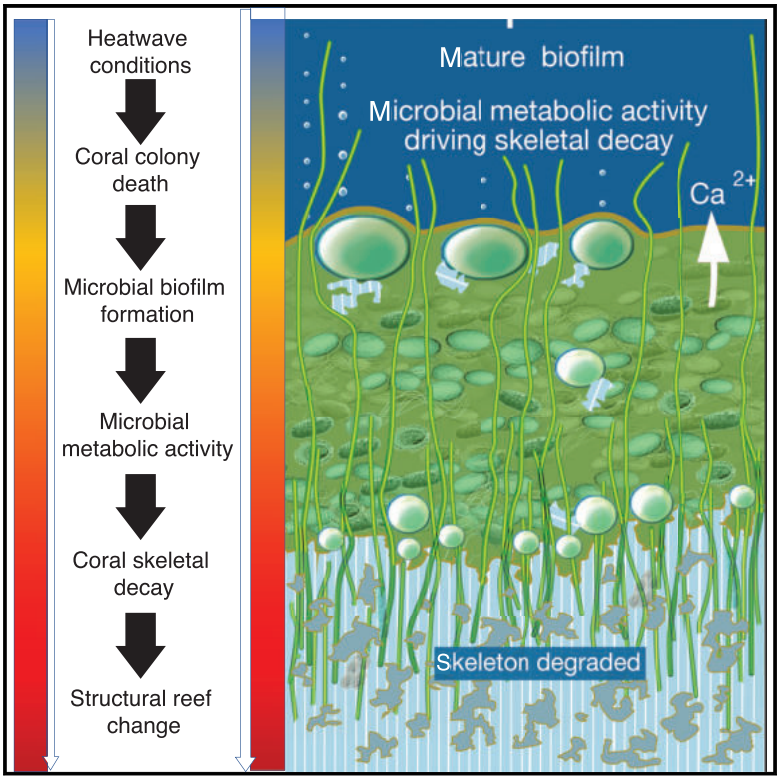

Highlights

- Marine heatwaves lead to rapid coral mortality and microbial biofilm formation
- Microbial metabolic activity results in rapid dissolution of the coral skeleton
- Dissolution reduces skeletal hardness and density and increased porosity

Authors

William P. Leggat, Emma F. Camp, David J. Suggett, ..., Unnikrishnan Kuzhiumparambil, C. Mark Eakin, Tracy D. Ainsworth

Correspondence

tracy.ainsworth@unsw.edu.au

In Brief

Due to climate change, coral reefs are now being subjected to extreme marine heatwave (MHW) conditions. Leggat et al. show that large-scale mortality due to MHWs and microbial colonization leads to a previously undescribed rapid dissolution of the coral skeleton.

Leggat et al., 2019, Current Biology *29*, 2723–2730
August 19, 2019
https://doi.org/10.1016/j.cub.2019.06.077

CellPress

Current Biology
Report

Rapid Coral Decay Is Associated with Marine Heatwave Mortality Events on Reefs

William P. Leggat,[1,2,8] Emma F. Camp,[3,8] David J. Suggett,[3,8] Scott F. Heron,[4,5,8] Alexander J. Fordyce,[1,2] Stephanie Gardner,[2,3] Lachlan Deakin,[6] Michael Turner,[6] Levi J. Beeching,[6] Unnikrishnan Kuzhiumparambil,[3] C. Mark Eakin,[5] and Tracy D. Ainsworth[2,7,8,9,*]

[1]School of Environmental and Life Sciences, University of Newcastle, Chittaway Road, Newcastle, NSW 2308, Australia
[2]Australian Research Council Centre of Excellence for Coral Reef Studies, James Cook University, University Drive, Townsville, QLD 4810, Australia
[3]Climate Change Cluster, University of Technology Sydney, PO Box 123, Broadway, NSW 2007, Australia
[4]Marine Geophysical Laboratory, Physics, College of Science and Engineering, James Cook University, University Drive, Townsville, QLD 4811, Australia
[5]Coral Reef Watch, U.S. National Oceanic and Atmospheric Administration, College Park, MD 20740, USA
[6]National Laboratory for X-Ray Micro Computed Tomography, Australian National University, Canberra, ACT 2610, Australia
[7]Biological, Earth and Environmental Sciences, University of New South Wales, Sydney, NSW 2052, Australia
[8]These authors contributed equally
[9]Lead Contact
*Correspondence: tracy.ainsworth@unsw.edu.au
https://doi.org/10.1016/j.cub.2019.06.077

SUMMARY

Severe marine heatwaves have recently become a common feature of global ocean conditions due to a rapidly changing climate [1, 2]. These increasingly severe thermal conditions are causing an unprecedented increase in the frequency and severity of mortality events in marine ecosystems, including on coral reefs [3]. The degradation of coral reefs will result in the collapse of ecosystem services that sustain over half a billion people globally [4, 5]. Here, we show that marine heatwave events on coral reefs are biologically distinct to how coral bleaching has been understood to date, in that heatwave conditions result in an immediate heat-induced mortality of the coral colony, rapid coral skeletal dissolution, and the loss of the three-dimensional reef structure. During heatwave-induced mortality, the coral skeletons exposed by tissue loss are, within days, encased by a complex biofilm of phototrophic microbes, whose metabolic activity accelerates calcium carbonate dissolution to rates exceeding accretion by healthy corals and far greater than has been documented on reefs under normal seawater conditions. This dissolution reduces the skeletal density and hardness and increases porosity. These results demonstrate that severe-heatwave-induced mortality events should be considered as a distinct biological phenomenon from bleaching events on coral reefs. We also suggest that such heatwave mortality events, and rapid reef decay, will become more frequent as the intensity of marine heatwaves increases and provides further compelling evidence for the need to mitigate climate change and instigate actions to reduce marine heatwaves.

RESULTS AND DISCUSSION

The benefits that are derived from coral reefs span from coastal protection to subsistence and industrial fisheries, and these benefits are indisputably contingent upon the integrity of the complex three-dimensional reef framework [4, 6]. In 2016, the Great Barrier Reef (GBR) experienced the most severe marine heatwave that has ever been recorded in the region [3]. Reefs of the northern GBR were exposed to severe sea surface temperatures (SSTs), in that 31% of GBR reefs experienced in excess of 8°C weeks (also referred to as 8-degree heating weeks [DHWs]) the established threshold for coral mortality [3, 7, 8]. Associated with this event, we observed a conspicuous weakening and erosion of the coral skeleton in corals exposed to the severe event on the northern GBR (Figures 1A–1D). We also found that the severe heat stress event in the northern GBR was exacerbated by the temporal development of the heating event, in that the sea surface temperature changes were characterized as a rapid and direct SST trajectory that has previously shown to result in high coral mortality [9] (Figures 1F and S1). A rapid degradation of the coral three-dimensional structure was observed *in situ* on the GBR (Figure 1D), and this occurred in the absence of any major storm or wave events (Figure S1). The loss of structure was also not consistent with mechanical damage (e.g., the breakage or tipping of colonies) but was apparent as an erosion of surface area and complexity of the coral colonies exposed to the rapid and severe heat stress. Further observations indicated a rapid colonization of exposed calcium carbonate skeleton by a microbial biofilm associated with the rapid coral mortality (Figures 1A–1D). Accompanying the formation of this biofilm was an apparent concurrent decay of the corals' calcium carbonate corallite structure (Figure 1D). Interestingly, severe heat stress events, wherein DHW exceeded

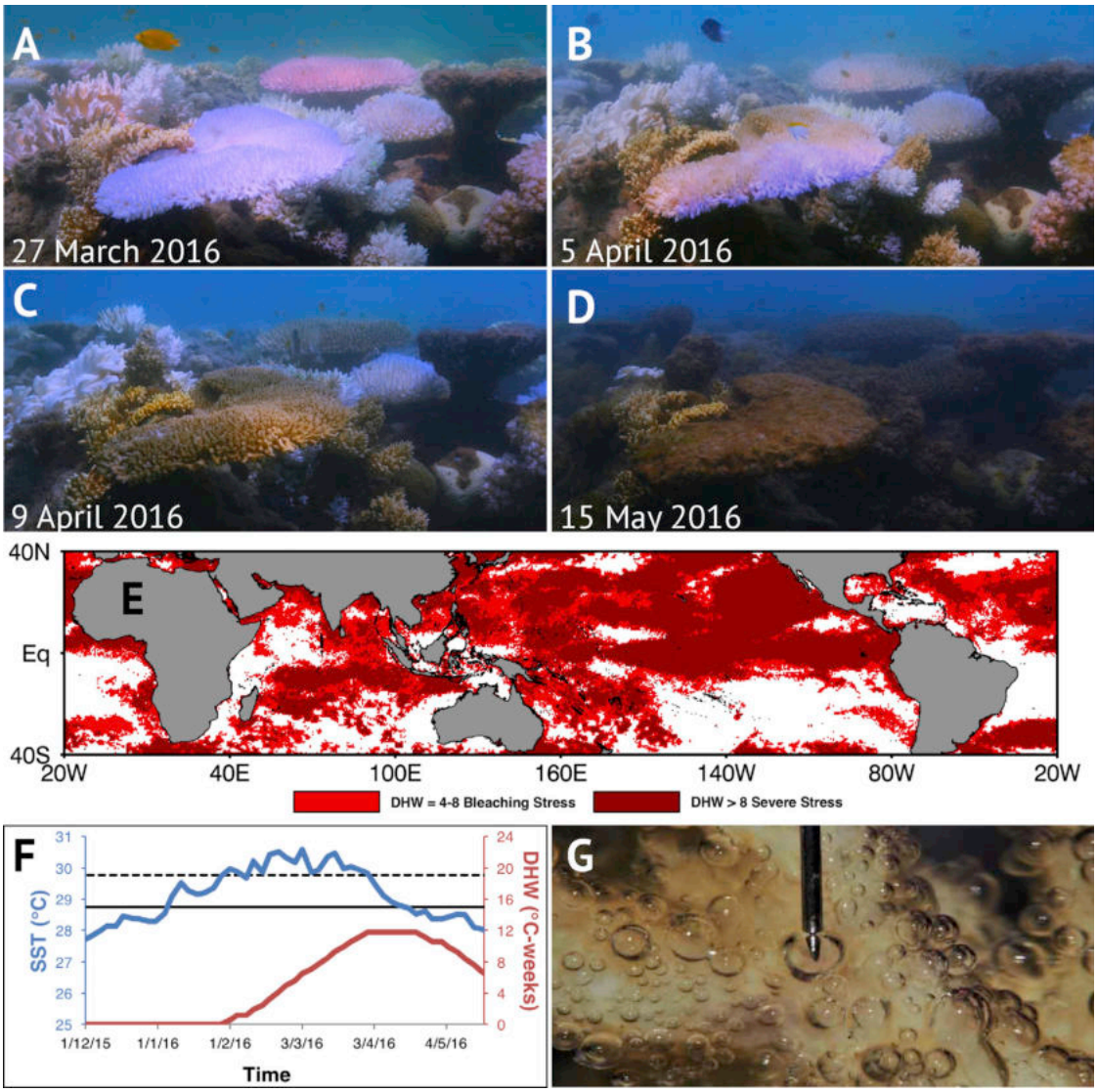

Figure 1. Responses of Northern GBR Corals to the Severe Marine Heatwave in 2016

(A–D) Time series of microbial colonization and succession following coral mortality over a 7 week period from March 27th (A) through April 5th (B), and April 9th (C) to May 15th (images from *Chasing Coral* [Netflix] courtesy of Exposure Labs).

(E) Worldwide distribution of bleaching level (DHW $\geq$ 4°C-weeks) and severe heat stress (DHW $\geq$ 8°C-weeks) during the period January 2014–May 2017, the latter threshold (dark red) indicating locations that have experienced marine heatwave conditions similar to those seen in the northern GBR in 2016.

(F) SST (blue) and DHW (red) experienced by northern GBR corals at Lizard Island.

(G) Microprobes were used to monitor microbial metabolism changes by measuring oxygen bubbles trapped within the biofilm during the light that rapidly developed on the coral skeleton post mortem.

See Figure S1.

8°C weeks, are not only evident in temperature records of the northern GBR from 2016 but in fact occurred on 37% of reef locations worldwide during the 2014–2017 widespread global coral-bleaching event (Figure 1E) [1], suggesting that these types of bleaching events are in fact a global phenomenon.

To investigate the drivers of the observed rapid coral skeletal decay, we simulated the severe heatwave conditions observed on the northern GBR during 2016. Two coral species that exhibited high mortality on GBR reefs in 2016 (*Pocillopora damicornis* and *Acropora aspera*) [3] were experimentally exposed to elevated SST conditions that resulted in not only the rapid loss of endosymbiotic dinoflagellates (bleaching) but also an immediate loss (heat-induced mortality) of the coral host tissue (Figures 2A, 2B, 2E, and 2F). Within our heatwave simulations, and consistent with field observations, the newly exposed calcium carbonate skeleton of heat-killed corals was rapidly colonized and encased by a complex microbial biofilm originating from the skeleton (within 2 days; Figures 2A–2H and S2; Video S1; Data S1 and S2). Utilizing fast repetition rate fluorescence (FRRf), we show there is an expansion of extant endolithic photoautotrophs within the coral skeleton and demonstrate the loss of photosynthetic signatures, characteristic of *Symbiodinium* spp., is followed

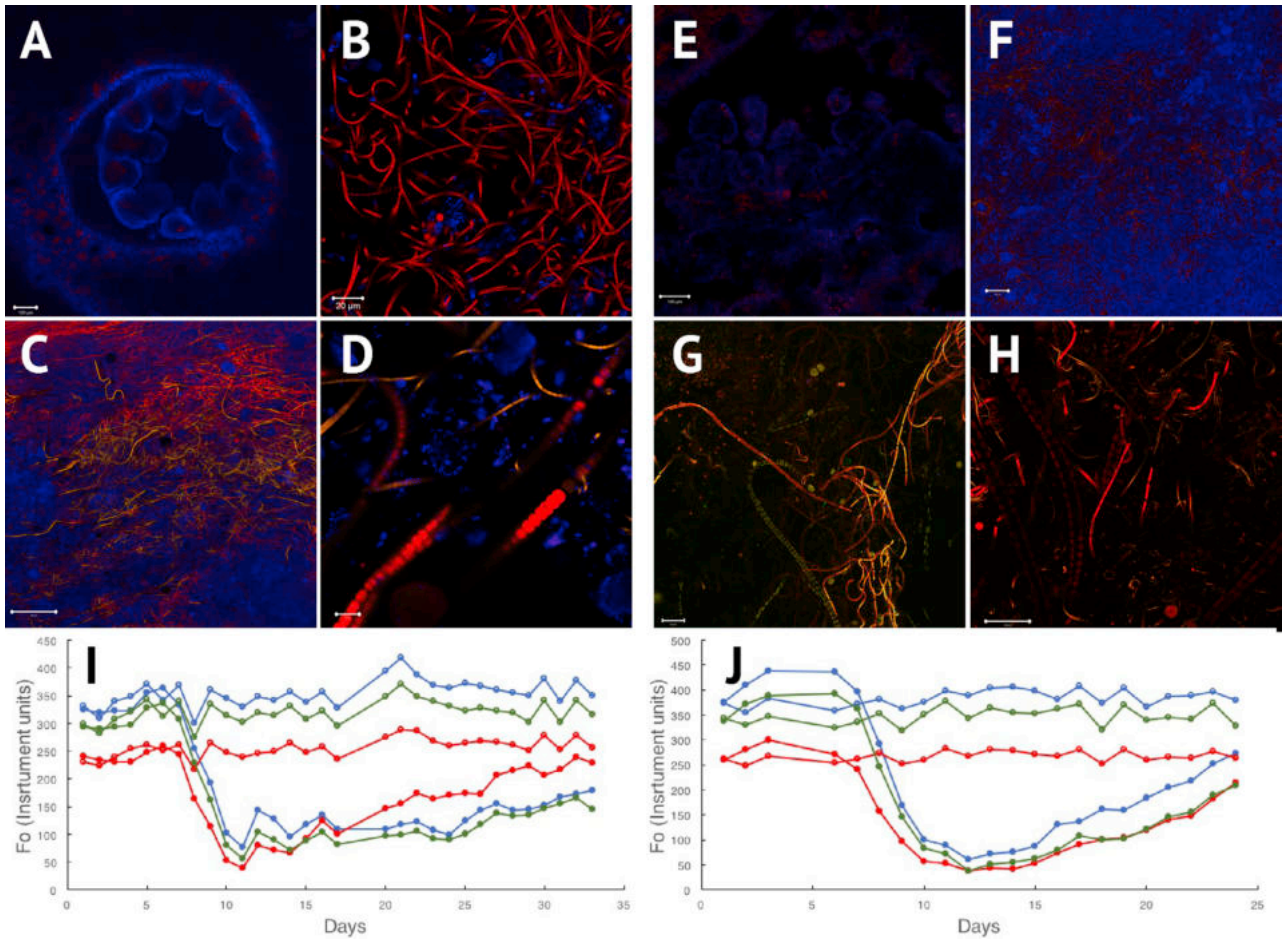

Figure 2. Microbial Biofilm Formation of *Pocillopora damicornis* and *Acropora aspera*

(A–H) Fluorescence images of healthy (A and E) and bleached (B and F) corals and the progression of microbial biofilm (C, D, G, and H) after heatwave-induced coral mortality of *P. damicornis* (A–D) and *A. aspera* (E–H) over a 6-week period (blue, coral tissue; red, photosynthetic algae). Scale bars for (A), (C), and (E)–(H) represent 100 μm, for (B) represent 20 μm, for (D) represent 10 μm.

(I and J) Multispectral FRR fluorescence for *P. damicornis* (I) and *A. aspera* (J) for healthy (open circles) and experimental coral (closed circles) at 450 nm (blue), 530 nm (green), and 625 nm (red).

See also Figures S2 and S3, Table S1, Data S1 and S2, and Video S1.

by an immediate increase of photosynthetic signatures of *Ostreobium* spp. and phycocyanin-containing cyanobacteria (Figures 2I, 2J, and S3). *Ostreobium* spp. is a green microalga globally prevalent in corals and found in high abundance within the skeleton below the corals organic matrix and polyp tissues [10]. A rapid population growth of *Ostreobium* spp. commonly occurs as a result of higher light penetration into the skeleton following coral bleaching, and where the bleached coral tissue remains intact following the loss of symbionts, this endolithic *Osteobium* spp. population is hypothesized to act as a beneficial symbiotic microbial association and provide a nutritional benefit to the coral through the provision of fixed carbon [11–15]. In the current study, the endolithic bloom was observed immediately after the loss of host tissues (i.e., following heat-induced tissue death and coral mortality) and was found to grow outward through the denuded coral polyp skeleton, and a complex biofilm encasing the coral skeleton was established (Figures 2C, 2D, 2G, 2H, and S3; Video S1; Data S1 and S2). In this case, the endolithic bloom was found to act as a colonizing microbe within the remaining coral skeleton, wherein increased light penetration of the skeleton likely enhanced growth of the otherwise light-limited endolithic community and, given the loss of intact coral tissues, no longer act as beneficial interaction for the host but as opportunistic overgrowth. The loss of the coral host tissues as a result of severe heat stress would in fact allow for a complete biofilm formation of the entire coral (within 1–3 days of the initiation of bleaching). We find that this biofilm was dominated by filamentous, chlorophyll-containing microalgae (genus *Ostreobium* spp.) and also colonizing Cyanobacteria (genera *Oscillotoria* spp. and *Anabaena* spp.), alongside a loss of the characteristic coral-associated Gammaproteobacteria. The overgrowing biofilm developed within 1 week of coral bleaching into a mixed population dominated by these filamentous chlorophyll-containing microbes (Figures 2 and S3). This is distinct to that which has been reported in bleached corals where the host remains intact, wherein the typical coral-bacterial associations remain, but the

bleached coral microbiome increases in diversity, and there is no reported increase in colonizing photo-autotrophs, as was found in the current study [16]. Importantly, filamentous *Ostreobium* spp. and cyanobacteria are both active chemical bioeroders of coral reef substrates, and the growth of these microbes is known to accelerate coral skeleton decay [17–19]. In addition, although processes, such as herbivory or scouring of the skeleton, which were not examined in this study, have the potential to modify or ameliorate the rate of biofilm formation, these would not alter the impact of heat-induced mortality of the host. Observations of large-scale coral mortality events occurring, and the extent of biofilm formation and colonization (as seen in Figure 1), indicate that algae removal processes are unlikely to effectively prevent the rapid biofilm formation that occurs during widespread heat-induced mortality and heatwave conditions (Figures 1A–1D).

Concerningly, we further show that *P. damicornis* and *A. aspera* skeletons encased by this microbial biofilm decalcified at rates of 1.9 ± 0.6 and 2.2 ± 0.7 μmol $Ca^{2+}/cm^{-2}/h^{-1}$ (mean ± SE), respectively (utilizing quantification of $CaCO_3$ accretion-dissolution through changes of free Ca^{2+} in surrounding seawater measured by microwave plasma-atomic emission spectrometry under ambient light intensity). Interestingly, $CaCO_3$ accretion-dissolution in darkness demonstrated the same trend as in the light, independent of species (Figures 3A and 3B). Importantly, the removal of the external biofilm did not significantly alter the decalcification rates, indicating internal microbial populations were contributing to the majority of decalcification (*P. damicornis*, $p = 0.177$; *A. aspera*, $p = 0.668$; Figures 3A and 3B). Corals of both species held within the replicate ambient (control) conditions remained healthy throughout the simulation period and exhibited significant growth within the experimental systems (post hoc sequential Bonferroni; $p < 0.001$), calcifying at respective rates of 1.7 ± 0.2 and 1.7 ± 0.3 μmol $Ca^{2+}.cm^{-2}.h^{-1}$ (Figures 3A and 3B). When converted to monthly rates, the dissolution values recorded here were more than 10 times found in a normal reef environment and more than 5 times higher than coral skeletal dissolution rates seen in extreme conditions (1,010 μatm pCO_2 with elevated temperatures; Table S1). The effect of this rapid dissolution can be seen in the field images from the 2016 bleaching event at Lizard Island (Figure 1) and further highlight the unique biological phenomena, caused by severe temperature and light conditions of marine heatwave events, on coral reefs, which we investigate in the current study (Figures 1A–1D).

Interestingly when exposed to heatwave conditions, microbial dissolution significantly altered the physical properties of the corals' calcium carbonate skeleton. Computer tomography (CT) scans [20] showed significant increases in total porosity (130%; $p = 0.038$) and micro-porosity (860%; $p = 0.006$) of biofilm-encased *P. damicornis* (Figure 3C) and total (53%; $p = 0.027$) and macro-porosity (107%; $p = 0.046$) in *A. aspera* (Figure 3D) over the 5-week simulation period. This increase in porosity also resulted in a significant loss (12% ± 1%; $p = 0.022$) of skeleton strength (hardness) for *P. damicornis* (Figure 3C). Consistent with increased porosity, skeletons of both *P. damicornis* and *A. aspera* also exhibited alterations to the ultrastructure and a loss of the characteristic calcium carbonate skeleton structure within 2 weeks of biofilm development (Figures 3E–3L and S4). Corals exhibited a widening of corallites and thinning of septa (Figures 3G, 3H, 3K, and 3L) when compared to healthy corals (Figures 3E, 3F, 3I, 3J, and S4). Similar microscale characteristic alterations have been reported as a result of decalcification in corals exposed to a high CO_2 environment [21]. Finally, we also find that oxygen bubbles trapped within the microbial biofilm immediately following coral mortality further signified a localized internal enhancement of microbial metabolism (Figure 1G). Microprobes confirmed a lower photosynthesis-to-respiration ratio (P:R) (mol O_2: mol O_2), driven by increased respiration over photosynthesis rates, inside the biofilm (*P. damicornis* = 1.35 ± 0.16; *A. aspera* = 0.56 ± 0.09) compared with healthy corals (*P. damicornis* = 1.76 ± 0.25; *A. aspera* = 1.02 ± 0.13). Increased respiration rates, and the associated increased CO_2 release, further accelerate chemical dissolution of the skeletal substrate, as reported in the current study. Although the exact mechanism by which microbial biofilm enhances dissolution could not be pinpointed, these responses are entirely consistent with metabolic acceleration of coral skeleton dissolution by *Ostreobium* spp. and cyanobacterial communities, as well as with heterotrophic bacterial breakdown of dissolved organic carbon from dead coral tissue [17, 22–24].

In conclusion, we propose that the rapid transition to microbial biofilm formation and skeletal decay that is associated with marine-heatwave-induced coral mortality, as reported here, is likely to become more common on coral reefs under future climate change (Figure 4). We suggest that further research into the frequency and severity of heatwave conditions on coral reefs is urgently needed; in particular, it is imperative to determine what conditions on reefs, such as mixing, water flow, and SST trajectory, have the potential to mitigate the speed of heat-induced mortality events. Information such as this may be critical in determining the effectivity of any local-scale interventions aiming to minimize coral mortality and retain reef-wide ecosystem function [25]. This research also highlights the need to re-think our understanding of coral bleaching and the immediate impact of climate change on coral reefs. Coral bleaching has been widely described, and modeled, as a process of symbiosis breakdown from which corals have the capacity to recover, via a re-uptake of endosymbionts, if elevated temperatures abate. Under these conditions, corals surviving the thermal stress event and subsequent bleaching process have the potential to acclimatize and adapt to thermal stress and predicted future SST increases [26]. However, here, we show that marine heatwave events on coral reefs are biologically distinct to how coral bleaching has been understood to date, in that heatwave conditions result in an immediate heat-induced mortality of the coral colony, rapid coral skeletal dissolution, and the loss of the three-dimensional reef structure.

Our results here, taken in context of underlying sea surface temperature conditions becoming more physiologically damaging within the coming decade [9] and climate models projections of severe coral bleaching exceeding 8°C-weeks DHW annually by 2030 [27], highlights the potential for bleaching events to have far more severe implications to the entire reef structure in the immediate future. Taken together, these results suggest far greater coral mortality associated with

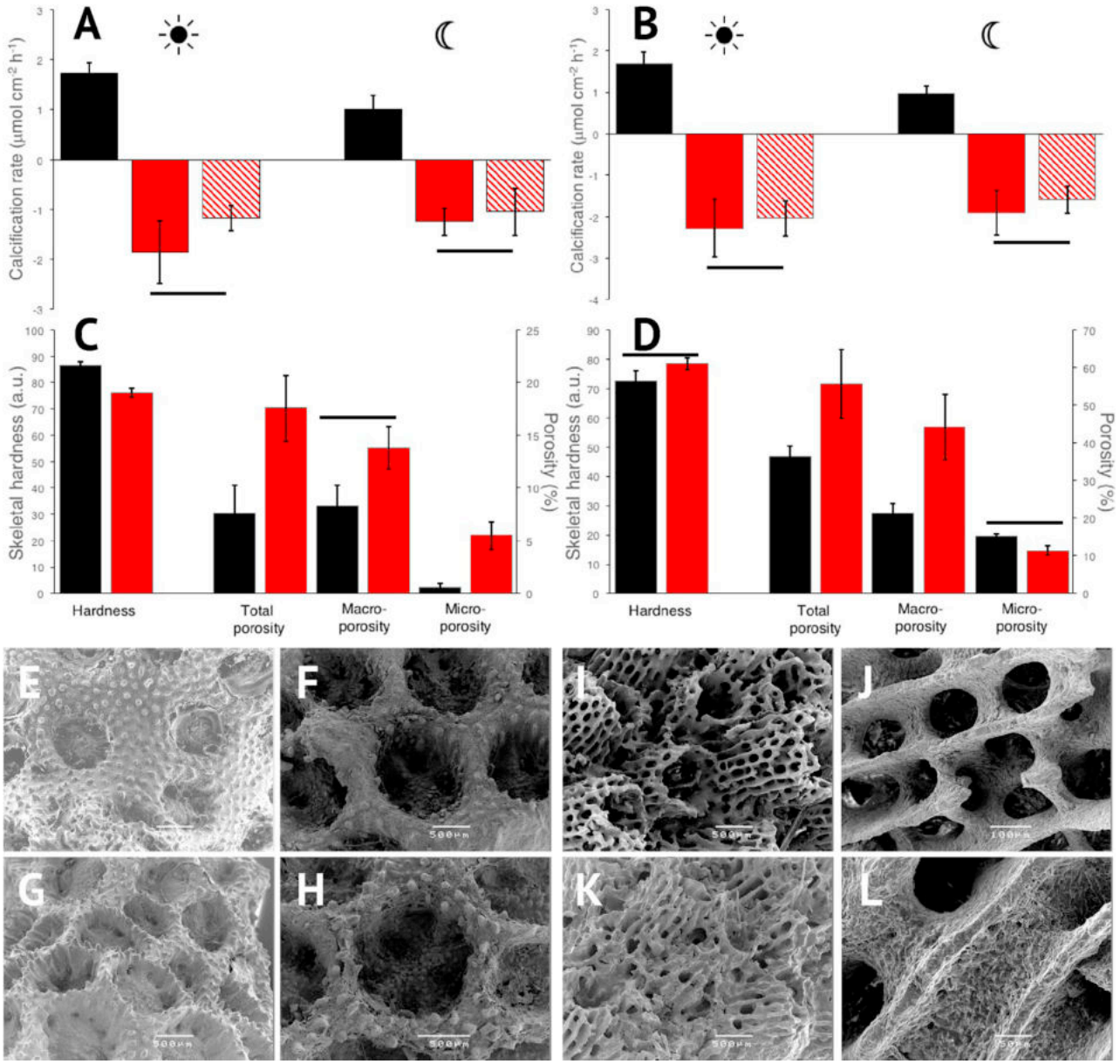

Figure 3. Skeletal Changes in *Pocillopora damicornis* and *Acropora aspera*

(A–D) Light and dark calcification rates for *P. damicornis* (A) and *A. aspera* (B) for healthy (black), algal overgrown (red), and algal overgrown with exterior biofilm removed (red hatched) corals 5 weeks after bleaching. Skeletal density and porosity of *P. damicornis* (C) and *A. aspera* (D), values represent average ± SE; n = 4; black, control; red, treatment. Bars cluster $p > 0.05$.

(E–L) Representative SEM images of *P. damicornis* (E–H) and *A. aspera* (I–L) corallites for healthy (E, F, I, and J) and biofilm-encased (G, H, K, and L) corals at the end of the simulation period. Scale bars for (E)–(I) and (K) represent 500 μm, for (J) represent 100 μm, and for (L) represent 50 μm.

See also Figures S2–S4, Data S1 and S2, and Video S1.

coral-bleaching events in the future. Our results also demonstrate that projected increases in SST have the potential to fuel the growth [17] and metabolic rates of microalgae and cyanobacteria during summer heatwaves, further enhancing the rate of microbial-driven coral dissolution [17, 28]. In fact, the reduction in structural complexity as documented here has already been observed as a result of the recent 2014–2017 global coral-bleaching event, where an approximately 30% reduction in topographic complexity was found in less than 1 year of the severe bleaching on two surveyed reefs [29]. Our evidence suggests erosion of coral skeletons is likely to occur far quicker than has so far been anticipated for coral reefs worldwide [30]. Such rapid decay starkly contrasts with previous estimates of erosion to the reef structural framework following bleaching, which is assumed to occur over timescales of months to years [29, 31–33]. Reef degradation is therefore likely to be an immediate

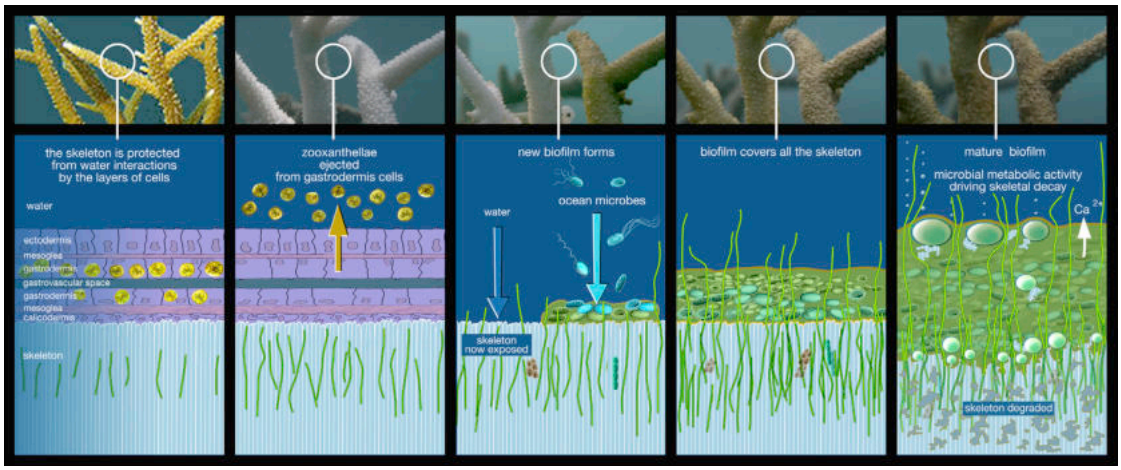

Figure 4. Schematic Representation of the Succession of Coral Dissolution following Marine Heatwaves
Coral fragments transition from healthy (left) to becoming encased by microbial biofilm (right) under severe heat stress, resulting in coral mortality, microbial colonization, and skeletal decay.

consequence of severe marine heatwave events on coral reefs, and concerningly, the implications of marine heatwaves on coral reefs globally have not yet been fully realized in predictions of future coral reef function [34].

The maintenance of the complex three-dimensional architecture of coral reefs is integral to sustaining ecological and socio-economic services of coral reefs in the immediate aftermath of anomalously high summer temperatures [6, 35, 36]. Our study provides compelling evidence for the urgent need for society to execute global and local efforts to mitigate climate change for the protection of coral reef ecosystems. A failure to mitigate climate change and minimize the emergence of frequent and severe marine heatwaves, as shown by Henson et al. [37], not only puts corals and coral reefs at risk of ecosystem collapse but also threatens the livelihoods of the half a billion people worldwide directly reliant on the goods and services they supply [38].

STAR★METHODS

Detailed methods are provided in the online version of this paper and include the following:

- KEY RESOURCES TABLE
- LEAD CONTACT AND MATERIALS AVAILABILITY
- EXPERIMENTAL MODEL AND SUBJECT DETAILS
- METHOD DETAILS
  - Observations at severe bleaching field site
  - Experimental simulation of extreme thermal heat stress conditions
  - Tissue Imaging
  - Biofilm microbial community profiling
  - Fast Repetition Rate (FRR) fluorescence monitoring of heat stress response of coral photosynthetic microbes
  - Calcium Chemistry
  - Scanning electron microscopy
  - CT Scan
  - Skeletal hardness analysis
- QUANTIFICATION AND STATISTICAL ANALYSIS
  - Microbiome Community Analysis
  - Statistical analysis
- DATA AND CODE AVAILABILITY

SUPPLEMENTAL INFORMATION

Supplemental Information can be found online at https://doi.org/10.1016/j.cub.2019.06.077.

ACKNOWLEDGMENTS

The authors would like to thank the following funding bodies: Australian Research Council, Centre of Excellence for Coral Reef Studies (CE0561435); Great Barrier Reef Foundation (Coral Health Grant); Australian Research Council Discovery Program Grant DP160100271 (D.S. and W.P.L.); NOAA NESDIS; and the NOAA Coral Reef Conservation Program. Sincere thanks to Exposure Labs for providing the images from *Chasing Coral* (Netflix). The contents in this manuscript are solely the opinions of the authors and do not constitute a statement of policy, decision, or position on behalf of NOAA or the U.S. Government. The authors would like to thank Professor Tony Larkum for initial identification of *Ostreobium sp*. and Mr. Levi Beaching (Australian National University, CT Laboratory), Professor Michael Cortie, and Ms. Christine Bligh for technical and laboratory assistance. Finally, the authors would like to thank the International Coral Reefs Society for their inspirational evening function at the 13th International Coral Reefs Symposium. The authors also thank Dr Ruth Gates for her support; forever admired, sorely missed, always an inspiration.

AUTHOR CONTRIBUTIONS

T.D.A., W.P.L., S.F.H., C.M.E., D.J.S., and E.F.C. designed the study. T.D.A., W.P.L., E.F.C., D.J.S., S.F.H., U.K., and A.J.F. conducted experimental procedures and physiological analyses. T.D.A., E.F.C., D.J.S., S.F.H., W.P.L., and C.M.E. wrote and finalized manuscript.

DECLARATION OF INTERESTS

The authors declare no competing interests.

Received: February 25, 2019
Revised: April 9, 2019
Accepted: June 25, 2019
Published: August 8, 2019

REFERENCES

1. Di Lorenzo, E., and Mantua, N. (2016). Multi-year persistence of the 2014/15 North Pacific marine heatwave. Nat. Clim. Chang. *6*, 1042–1047.
2. Oliver, E.C.J., Donat, M.G., Burrows, M.T., Moore, P.J., Smale, D.A., Alexander, L.V., Benthuysen, J.A., Feng, M., Sen Gupta, A., Hobday, A.J., et al. (2018). Longer and more frequent marine heatwaves over the past century. Nat. Commun. *9*, 1324.
3. Hughes, T.P., Kerry, J.T., Álvarez-Noriega, M., Álvarez-Romero, J.G., Anderson, K.D., Baird, A.H., Babcock, R.C., Beger, M., Bellwood, D.R., Berkelmans, R., et al. (2017). Global warming and recurrent mass bleaching of corals. Nature *543*, 373–377.
4. Graham, N.A.J., and Nash, K.L. (2013). The importance of structural complexity in coral reef ecosystems. Coral Reefs *32*, 315–326.
5. Graham, N.A.J., Cinner, J.E., Norström, A.V., and Nyström, M. (2014). Coral reefs as novel ecosystems: embracing new futures. Curr. Opin. Environ. Sustain. *7*, 9–14.
6. Ferrario, F., Beck, M.W., Storlazzi, C.D., Micheli, F., Shepard, C.C., and Airoldi, L. (2014). The effectiveness of coral reefs for coastal hazard risk reduction and adaptation. Nat. Commun. *5*, 3794.
7. Liu, G., Heron, S.F., Eakin, C.M., Muller-Karger, F.E., Vega-Rodriguez, M., Guild, L.S., De La Cour, J.L., Geiger, E.F., Skirving, W.J., Burgess, T.F.R., et al. (2014). Reef-scale thermal stress monitoring of coral ecosystems: new 5-km global products from NOAA coral reef watch. Remote Sens. *6*, 11579–11606.
8. Eakin, C.M., Morgan, J.A., Heron, S.F., Smith, T.B., Liu, G., Alvarez-Filip, L., Baca, B., Bartels, E., Bastidas, C., Bouchon, C., et al. (2010). Caribbean corals in crisis: record thermal stress, bleaching, and mortality in 2005. PLoS ONE *5*, e13969.
9. Ainsworth, T.D., Heron, S.F., Ortiz, J.C., Mumby, P.J., Grech, A., Ogawa, D., Eakin, C.M., and Leggat, W. (2016). Climate change disables coral bleaching protection on the Great Barrier Reef. Science *352*, 338–342.
10. Del Campo, J., Pombert, J.F., Šlapeta, J., Larkum, A., and Keeling, P.J. (2017). The 'other' coral symbiont: ostreobium diversity and distribution. ISME J. *11*, 296–299.
11. Littman, R., Willis, B.L., and Bourne, D.G. (2011). Metagenomic analysis of the coral holobiont during a natural bleaching event on the Great Barrier Reef. Environ. Microbiol. Rep. *3*, 651–660.
12. Fine, M., Steindler, L., and Loya, Y. (2004). Endolithic algae photoacclimate to increased irradiance during coral bleaching. Mar. Freshw. Res. *55*, 115–121.
13. Fine, M., Roff, G., Ainsworth, T.D., and Hoegh-Guldberg, O. (2006). Phototrophic microendoliths bloom during coral "white syndrome". Coral Reefs *25*, 577–581.
14. Fine, M., and Loya, Y. (2002). Endolithic algae: an alternative source of photoassimilates during coral bleaching. Proc. Biol. Sci. *269*, 1205–1210.
15. Fine, M., Meroz-Fine, E., and Hoegh-Guldberg, O. (2005). Tolerance of endolithic algae to elevated temperature and light in the coral Montipora monasteriata from the southern Great Barrier Reef. J. Exp. Biol. *208*, 75–81.
16. Gardner, S.G., Camp, E.F., Smith, D.J., Kahlke, T., Osman, E.O., Gendron, G., Hume, B.C.C., Pogoreutz, C., Voolstra, C.R., and Suggett, D.J. (2019). Coral microbiome diversity reflects mass coral bleaching susceptibility during the 2016 El Niño heat wave. Ecol. Evol. *9*, 938–956.
17. Reyes-Nivia, C., Diaz-Pulido, G., Kline, D., Guldberg, O.H., and Dove, S. (2013). Ocean acidification and warming scenarios increase microbioerosion of coral skeletons. Glob. Change Biol. *19*, 1919–1929.
18. Tribollet, A. (2008). The boring microflora in modern coral reef ecosystems: a review of its roles. In Current Developments in Bioerosion, M. Wisshak, and L. Tapanila, eds. (Springer), pp. 67–94.
19. Schönberg, C.H.L., Fang, J.K.H., Carreiro-Silva, M., Tribollet, A., and Wisshak, M. (2017). Bioerosion: the other ocean acidification problem. ICES J. Mar. Sci. *74*, 895–925.
20. Varslot, T., Kingston, A., Myers, G., and Sheppard, A. (2011). High-resolution helical cone-beam micro-CT with theoretically-exact reconstruction from experimental data. Med. Phys. *38*, 5459–5476.
21. Enochs, I.C., Manzello, D.P., Kolodziej, G., Noonan, S.H.C., Valentino, L., and Fabricius, K.E. (2016). Enhanced macroboring and depressed calcification drive net dissolution at high-CO2 coral reefs. Proc. Roy. Soc. B: Biol. Sci. *283*, 20161742.
22. Ramírez-Reinat, E.L., and Garcia-Pichel, F. (2012). Characterization of a marine cyanobacterium that bores into carbonates and the redescription of the genus mastigocoleus(1). J. Phycol. *48*, 740–749.
23. Garcia-Pichel, F., Ramírez-Reinat, E., and Gao, Q. (2010). Microbial excavation of solid carbonates powered by P-type ATPase-mediated transcellular Ca^{2+} transport. Proc. Natl. Acad. Sci. USA *107*, 21749–21754.
24. Kline, D.I., Kuntz, N.M., Breitbart, M., Knowlton, N., and Rohwer, F. (2006). Role of elevated organic carbon levels and microbial activity in coral mortality. Mar. Ecol. Prog. Ser. *314*, 119–125.
25. McDonald, J., McGee, J., Brent, K., and Burns, W. (2019). Governing geoengineering research for the Great Barrier Reef. Clim. Policy *19*, 801–811.
26. Palumbi, S.R., Barshis, D.J., Traylor-Knowles, N., and Bay, R.A. (2014). Mechanisms of reef coral resistance to future climate change. Science *344*, 895–898.
27. van Hooidonk, R., Maynard, J.A., and Planes, S. (2013). Temporary refugia for coral reefs in a warming world. Nat. Clim. Chang. *3*, 508–511.
28. Tribollet, A., Godinot, C., Atkinson, M., and Langdon, C. (2009). Effects of elevated pCO_2 on dissolution of coral carbonates by microbial euendoliths. Global Biogeochem. Cycles *23*, GB3008.
29. Couch, C.S., Burns, J.H.R., Liu, G., Steward, K., Gutlay, T.N., Kenyon, J., Eakin, C.M., and Kosaki, R.K. (2017). Mass coral bleaching due to unprecedented marine heatwave in Papahānaumokuākea Marine National Monument (Northwestern Hawaiian Islands). PLoS ONE *12*, e0185121.
30. Frieler, K., Meinshausen, M., Golly, A., Mengel, M., Lebek, K., Donner, S.D., and Hoegh-Guldberg, O. (2013). Limiting global warming to 2°C is unlikely to save most coral reefs. Nat. Clim. Chang. *3*, 165–170.
31. Alvarez-Filip, L., Dulvy, N.K., Gill, J.A., Côté, I.M., and Watkinson, A.R. (2009). Flattening of Caribbean coral reefs: region-wide declines in architectural complexity. Proc. Biol. Sci. *276*, 3019–3025.
32. Eakin, C.M. (1996). Where have all the carbonates gone? A model comparison of calcium carbonate budgets before and after the 1982–1983 El Nino at Uva Island in the eastern Pacific. Coral Reefs *15*, 109–119.
33. Eakin, C.M. (2001). A tale of two ENSO events: carbonate budgets and the influence of two warming disturbances and intervening variability, Uva Island, Panama. Bull. Mar. Sci. *69*, 171–186.
34. Logan, C.A., Dunne, J.P., Eakin, C.M., and Donner, S.D. (2014). Incorporating adaptive responses into future projections of coral bleaching. Glob. Change Biol. *20*, 125–139.
35. Hobday, A.J., Cochrane, K., Downey-Breedt, N., Howard, J., Aswani, S., Byfield, V., Duggan, G., Duna, E., Dutra, L.X.C., Frusher, S.D., et al. (2016). Planning adaptation to climate change in fast-warming marine regions with seafood-dependent coastal communities. Rev. Fish Biol. Fish. *26*, 249–264.
36. Sobel, A.H., Camargo, S.J., Hall, T.M., Lee, C.Y., Tippett, M.K., and Wing, A.A. (2016). Human influence on tropical cyclone intensity. Science *353*, 242–246.
37. Henson, S.A., Beaulieu, C., Ilyina, T., John, J.G., Long, M., Séférian, R., Tjiputra, J., and Sarmiento, J.L. (2017). Rapid emergence of climate change in environmental drivers of marine ecosystems. Nat. Commun. *8*, 14682.
38. Pendleton, L., Comte, A., Langdon, C., Ekstrom, J.A., Cooley, S.R., Suatoni, L., Beck, M.W., Brander, L.M., Burke, L., Cinner, J.E., et al. (2016). Coral reefs and people in a high-CO2 world: where can science make a difference to people? PLoS ONE *11*, e0164699.

39. Caporaso, J.G., Kuczynski, J., Stombaugh, J., Bittinger, K., Bushman, F.D., Costello, E.K., Fierer, N., Peña, A.G., Goodrich, J.K., Gordon, J.I., et al. (2010). QIIME allows analysis of high-throughput community sequencing data. Nat. Methods *7*, 335–336.

40. Heron, S.F., Liu, G., Rauenzahn, J.L., Christensen, T.R.L., Skirving, W.J., Burgess, T.F.R., Eakin, C.M., and Morgan, J.A. (2014). Improvements to and continuity of operational global thermal stress monitoring for coral bleaching. Journal of Operational Oceanography *7*, 3–11.

41. Puotinen, M., Maynard, J.A., Beeden, R., Radford, B., and Williams, G.J. (2016). A robust operational model for predicting where tropical cyclone waves damage coral reefs. Sci. Rep. *6*, 26009.

42. Holcomb, M., Cohen, A.L., Gabitov, R.I., and Hutter, J.L. (2009). Compositional and morphological features of aragonite precipitated experimentally from seawater and biogenically by corals. Geochim. Cosmochim. Acta *73*, 4166–4179.

STAR★METHODS

KEY RESOURCES TABLE

REAGENT or RESOURCE	SOURCE	IDENTIFIER
Critical Commercial Assays		
AmpliTaq Gold 360 mastermix	Life Technologies, Australia	https://www.thermofisher.com/au/en/home/brands/life-technologies.html
TaKaRa Taq DNA Polymerase	Clontech	https://www.takarabio.com
Picogreen	Invitrogen	https://www.google.com/search?client=safari&rls=en&q=invitrogen&ie=UTF-8&oe=UTF-8
Deposited Data		
All figures and corresponding metadata are available at FigShare	This paper	https://doi.org/10.6084/m9.figshare.4867415
16 s sequence data	This paper	NCBI BioProject: PRJNA540757
Code for analysis of SST	NOAA - Coral Reef Watch	https://coralreefwatch.noaa.gov/
GreenGenes	Lawrence Livermore National Laboratory and Lawrence Berkeley National Laboratory	https://greengenes.secondgenome.com
Software and Algorithms		
SPSS Statistics	IBM Corporation	Version 24
QIIME	[39]	http://qiime.org
Other		
Microwave plasma-atomic emission spectrometer	Agilent, USA	MP-AES 4100
Scanning Electron Microscope	Jeol, Frenchs Forest NSW 2086 Australia	JSM5410LV
Multispectral FRR flourometer	FastOcean, Chelsea Technologies Group, UK	https://www.chelsea.co.uk/fast-ocean-apd-profiling-system
Illumina MiSeq	Illumina San Diego, CA, USA	https://www.illumina.com/

LEAD CONTACT AND MATERIALS AVAILABILITY

Requests for an information, resources or reagents should be directed to and will be fulfilled by the Lead Contact Tracy Ainsworth (tracy.ainsworth@unsw.edu.au).

EXPERIMENTAL MODEL AND SUBJECT DETAILS

Pocillopora damicornis colonies (approximately 10 cm in diameter) (n = 32 colonies divided into quarters to generate 128 fragments; parent colony was annotated per sample and each parent colony fragment was assigned to unique analysis to prevent pseudo-replication) and *Acropora aspera* nubbins (8-10 cm long) (160 fragments collected from at 6 distinct colonies separated by at least 10 m) were collected from the reef flat of Heron Island, Australia (23.4423°S, 151.9148°E) in January 2017, and were randomly allocated to one of four flow-through raceways (approximately 1000 L each) (see schematic Figure S2B).

METHOD DETAILS

Observations at severe bleaching field site

Time-lapse footage of coral bleaching, mortality and degradation from Lizard Island, Australia (14.67933°S, 145.446°E) was collected by Exposure Labs from 9th March until 15th May 2016. Temperature analysis was undertaken at 0.5° (~50 km) resolution using the Coral Reef Watch (CRW) Contingency SST produce, which became the primary data source for CRW's 0.5° products on 1st February 2016 (i.e., during the studied heat stress event). These data were used to analyze the SST time-series and derive data products. Reef-containing pixels (n = 1928) were defined using the ReefBase reef locations dataset and following Heron et al. [40]. Wind speed data for Lizard Island were acquired from the satellite-derived Blended SeaWinds 0.25°, daily dataset. Monthly climatological wind speed

and variability were determined from the period July 1987-April 2017, and used to consider potential reef degradation related to high wind (storm) events during the period of observations. During the footage acquisition, the only wind speed event to exceed the climatological value by more than two standard deviations (SD) coincided with the peak of bleaching (14th March, Figure S1), before structural degradation was seen. Notably, the only wind speed event greater than the gale force threshold (17 m/s = 34 kts;) occurred on 19th May, after the observation of structural degradation. Significant wave heights (H_s) for Lizard Island from the WaveWatch III model (0.5°, 3-hourly) for the period February 2005-December 2016 were similarly examined to also consider effects of longer period waves (swell) generated by distant weather systems. Wave height exceeded the climatological value by more than two SD only once during the footage acquisition (25th April, 0300 hr UTC; Figure S1); however, neither this nor any other wave event reached the threshold required for the waves to cause mechanical significant damage to corals ($H_s \geq 4$ m) [41]. Importantly for both wind and wave conditions, the corals studied were inside the lagoon, thereby protected from any broad-scale impacts and with limited fetch for the development of damaging sea conditions. That no broad-scale events occurred during the period of footage acquisition indicates that it is very unlikely that structural degradation was associated with external physical impacts. Corals were also collected from sites within the Northern Great Barrier Reef exposed to these severe conditions for tissue biopsies and symbiont density as a means to determine the extent of the bleaching during the event. The collected corals were observed to be extremely weak, break easily upon handling, and be colonized by micro-algae (personal observations of authors Ainsworth, Leggat). Taken together these *in situ* observations of the 2016 heat-wave provided the impetus for the current study to undertake a simulation of the severe marine heat-wave conditions. SST conditions during the 2016 marine heatwave (Figure S1) and previous summertime periods linked to bleaching conditions in the region (Figure S1) were also investigated, with 2016 marine heatwave found to be more severe than past bleaching events, these thermal profiles were used for experimental simulation of marine heatwaves.

Experimental simulation of extreme thermal heat stress conditions

Each pair of raceways (control and treatment) was fed from a sump tank (3000 L), which was supplied with water from the reef flat. Coral nubbins (*P. damicornis* and *A. aspera)* were allowed to acclimatize for one week and were assigned to two thermal treatment raceways and two ambient raceways, the thermal treatment corals subjected to a simulated bleaching event, heating was controlled throughout the experiment by heating the sump tanks using two 3 kW submersible, programable, titanium heaters (Aquasonic, Australia). Elevated temperatures were maintained throughout the peak light/temperature conditions by daily ramping beginning at 9am, peak daily temperatures occurring mid-day and cooling occurring through the afternoons with overnight relaxation of temperatures. Each day temperature was increased approximately 1 degree from the previous day until the peak thermal exposure at the bleaching threshold (34°C for these corals on the heron island reef flat) over several days. Thermal variance was simulated based on reef conditions experienced on Lizard Island during the 2016 bleaching event (please see Figures S1 and S2). Water flow was maintained throughout the experimental period at approximately 0.05 m per second within all the experimental raceways. Each coral fragment was imaged every 2 days throughout the experimental period and images are provided as supplementary image files (Data S1 and S2) and changes to coral buoyancy at the end of the experimental period were video recorded (Video S1). In the experimental systems alkalinity was recorded at 2306 μm/kg seawater (+/−7) (control) and 2311 (+/−7) (treatment); salinity was recorded at 34.7 ppt (+/−0.05) (controls) and 34.9 ppt (+/−0.07). pH was recorded twice daily in all experimental tanks and was found to range between 7.9 - 8.2, consistent with previous records for the reef flat environment at Heron Island.

Tissue Imaging

The coral biofilm was dissected from the coral skeleton to allow wholemount imaging. The biofilm was suspended in DNA/RNA free water in a cover glass bottomed Petri dish and innate fluorescence was imaged on a Zeiss Confocal Microscope under 10X magnification, excitation using 488, 561, 633 lasers, fluorescence emission was collected in 9.2nm bands between 488 and 700nm. The biofilm was also imaged via Z stacking (70-100 optical slices per polyp) and 3D images were constructed using Zeiss Zen 2009 imaging software.

Biofilm microbial community profiling

DNA was extracted from the biofilm of bleached and healthy coral skeletons. PCR amplification and sequencing was performed by the Australian Genome Research Facility. The 16S rRNA gene PCR primers 27F/519R with barcode on the forward primer were used in a PCR under the following conditions; 29 cycles of 95°C for 7 minutes, 94°C for 45 s, 50°C for 60 s, 72°C for 60 s, 73°C for 7 minutes. AmpliTaq Gold 360 mastermix (Life Technologies, Australia) for the primary PCR. A secondary PCR to index the amplicons was performed with TaKaRa Taq DNA Polymerase (Clontech). The resulting amplicons were measured by fluorometry (Invitrogen Picogreen) and normalized. The eqimolar pool was then measured by qPCR (KAPA) followed by sequencing on the Illumina MiSeq (San Diego, CA, USA) with 2 × 300 base pairs paired-end chemistry. DNA yield was recorded for all samples, DNA amplification was attempted for all samples and failure to amplify DNA was recorded.

Fast Repetition Rate (FRR) fluorescence monitoring of heat stress response of coral photosynthetic microbes

Active fluorometry was used daily to evaluate the physiological response of all control and heat stress coral nubbins throughout the experiment. A multispectral FRR flourometer (*FastOcean*, Chelsea Technologies Group, UK) was used to discriminate the responses of different photosynthetic microbial pigment groups during heat stress and subsequent biofilm development. We employed the same set up of housing corals within the open optical head of an FRRf. All nubbins were measured at 08:00 local time by initially acclimating nubbins to low light. The FRRf was programmed to deliver single turnover chlorophyll fluorescence induction curves using

LED excitation of different colors (blue, 450nm, green, 530nm, and orange 625nm), to preferentially stimulate chromophytes (e.g., *Symbiodinium* spp., FI-ex: 450 > 530 > 625), chlorophytes (e.g., Ostreobium spp., FI-ex: 450 > 625 > 530) and phycocyanin-containing cyanobacteria (e.g., Anabaena spp., FI-ex: 625 > 530 > 450), respectively. A model was fit to each induction curve to retrieve physiological terms, including the fluorescence yield (F_0, instrument units), and maximum photochemical efficiency (F_v/F_m, dimensionless). Photophysiological responses for *A. aspera* were similar to those for *P. damicornis*, with the exception that heat stressed fragments show a switch from the *Symbiodinium* community (days 10-13) to the biofilm development, as a cumulative dominance of F_0 (625, 450) over F_0 (530) primarily through growth of *Ostreobium* spp. Loss of F_v/F_m from heat stress (Days 8-11) exhibited a slower 'recovery' to initial values but again reflecting active growth through a switch in microbial assemblage. Trends show maintenance of F_0 (450 > 530 > 625) in control fragments throughout the experimental period, as expected for an intact coral where the photosynthetic community is dominated by *Symbiodinium* spp. Heat stress-treatment fragments show a switch from the *Symbiodinium* community (days 0-7) to the biofilm development, as a cumulative dominance of F_0 (625) over F_0 (450, 530) of a mixed assemblage of *Anabaena* and *Ostreobium* spp. Loss of F_v/F_m from heat stress was transient (Days 8-11) and recovers to initial values reflecting active growth but through a switch in microbial assemblage.

Calcium Chemistry

Analysis of calcium was performed using a microwave plasma-atomic emission spectrometer (Agilent MP-AES 4100, USA) equipped with a concentric nebulizer and a double pass cyclonic spray chamber. Sea water samples were digested with concentrated nitric acid for 1h and were filtered from 0.45 μm syringe mounted filter. Digests were further diluted with 2% nitric acid solution and quantified for calcium ion by external standard method (R^2 = 0.999). For the highest sensitivity, nebulizer pressure and viewing position were optimized automatically by the instrument. Before every sample reading, 30 s of uptake time and 30 s of torch stabilization time were set. Emission measurements were done at wavelengths, 422.67 nm and 393.36 nm and for each sample, 5 s read time with 3 replicates were applied. Precision and accuracy of the method was validated using replicate analysis of spiked samples. The recovery obtained was between 90.5 to 106.3%, with a precision of < 4% RSD.

Scanning electron microscopy

A 2 cm wide cross-section was taken from the mid-point of the 7 cm coral branch. The cross-sections of coral skeletons were then washed in freshwater, the coral tissues and biofilm were removed with gentle brushing, and the skeletons allowed to dry overnight prior to mounting on stainless steel disks. Each cross-section was mounted to allow for imaging of the polyp structure on the outer surface of the coral skeleton and the skeleton was coated in 99.5% pure gold. Samples of healthy control corals (n = 4 per species per time point, for 3 time points), thermally exposed corals (n = 4 per species per time point, for 3 time points) and wild collected corals (n = 4) were imaged using a Jeol JSM5410LV.

CT Scan

CT scanning was used to determine micro-, macro-, and total porosity of skeletons from biofilm encased and healthy corals. Each sample image (n = 2 coral skeletons per experimental tank, per treatment per species) was acquired with a double helical trajectory on an FEI HeliScan MicroCT and reconstructed at 26.2 μm. A variant of the flood fill algorithm with a constrained invasion radius was used to mask the external empty space in the image. The images were segmented into pore, solid, and sub-resolution porosity (micro-porosity) phases using a converging active contours algorithm. The contribution of sub-resolution porosity to the total porosity was estimated based on local voxel intensity. All associated methods and algorithms are available through collaboration with the National Laboratory for X-ray Micro Computed Tomography, Australian National University, Australia.

Skeletal hardness analysis

A 1 cm cross section of coral was taken 4 cm down from the newest growth point of each fragment (n = 5 per treatment, per species). Cross sections were embedded in resin and polished [42], before micro-hardness (6-8 replicate measurements per cross-section) was assessed using a Model D Shore scleroscope, calibrated on reference material and optimized for natural rock as outlined by International Society for Rock Mechanics (ISRM, 2014). With this technique, hardness is determined by the rebound height of the diamond tipped hammer, by its own weight and from a fixed height. It is measured on a calibrated scale which gives the Shore hardness value (SH) in its own units, with higher values indicated a harder material.

QUANTIFICATION AND STATISTICAL ANALYSIS

Microbiome Community Analysis

Sequences were joined, depleted of barcodes then sequences < 150bp removed, sequences with ambiguous base calls removed, sequences were denoised, OTUs generated, and chimeras removed, sequence data was processed and analyzed utilizing the open source Quantitative Insights into Microbial Ecology (QIIME) [39]. Operational taxonomic units (OTUs) were defined by clustering at 3% divergence (97% similarity). Final OTUs were taxonomically classified using BLASTn against a curated database derived from GreenGenes, RDPII and NCBI. Sequence data is openly available via Figshare https://doi.org/10.6084/m9.figshare.4867415 and at NCBI (GeneBank BioProject ID: PRJNA540757) or directly through the authors (bill.leggat@newcastle.edu.au). A microbiome dataset consisting of 69,194 sequences per sample (total of 968724 sequences) was subsequently generated and used in the following

analyses. Analysis of the 16 s rDNA of healthy and biofilm encased *P. damicornis* at the end of the experimental period show distinct differences in the bacterial population. The population of the biofilm encased corals are dominated by cyanobacteria (45% ± 5%), with the majority being from the family Pseudanabaenaceae (34.4%), with one taxon making up 10% ± 2% of the bacterial population. In contrast in healthy coral this family only comprised 5.3% of the bacterial population. The next most abundance group in biofilm encased *P. damicornis* are Alphaproteobacteria (35% ± 4%), which are dominated by one OTU (10% ± 2%) with no close match in available databases. In healthy corals this OTU represents only 1.3% ± 0.5% of the bacterial population.

Statistical analysis

Data for the calcium chemistry, skeletal hardness, oxygen measurements, microporosity, macroporosity and total porosity were analyzed using SPSS Statistics (v24, IBM Corp.) using an ANOVA with temperature a mains effect and tank a random effect.

DATA AND CODE AVAILABILITY

All figures and corresponding metadata are available via FigShare https://doi.org/10.6084/m9.figshare.4867415 and can be provided directly via contact with the authors (tracy.ainsworth@unsw.edu.au, bill.leggat@newcastle.edu.au, emma.camp@uts.edu.au). Code for the analysis of SST data and the raw SST data are available from https://coralreefwatch.noaa.gov/. Methods and algorithms for the Computed Tomography (CT) scanning are available through collaboration with the National Laboratory for X-ray Micro Computed Tomography, Australian National University, Australia. 16 s sequence data is available at NCBI under BioProject ID: PRJNA540757 or directly through the authors (bill.leggat@newcastle.edu.au).